High-speed time series prediction and classification on an all-optical neural network

Aashu Jha[1,*], Chaoran Huang[1,2], Hsuan-Tung Peng[1], Weipeng Zhang[1], Bhavin Shastri[1,3], Paul R. Prucnal[1]

1. Lightwave Communications Research Laboratory, Department of Electrical Engineering Princeton University, Princeton, NJ, 08544 USA
2. Department of Electronic Engineering, Chinese University of Hong Kong, Hong Kong
3. Department of Physics, Engineering Physics Astronomy, Queen's University, Kingston ON, K7L 3N6, Canada
** aashuj@princeton.edu*

Abstract: We experimentally demonstrate high-speed time series prediction and binary classification tasks using an all-optical integrated SiN-based nonlinear photonic node in a time-delay based reservoir architecture.

1. Introduction

The primary incentives of photonic computing are high speed and low latency, which can most easily be achieved with a passive, all-optical hardware and a small network. Nonlinear photonic effects can be utilized for all-optical processing and a time-delay based reservoir architecture constrains the network size. Ref. [1] introduced time-delay based reservoirs which utilize a single dynamical nonlinear node with delayed feedback as the reservoir. The combination of all-optical nonlinearity and reservoir utilizes both the high-speed, low latency of photonic processing as well as the relative ease of training and reduction in hardware overhead in reservoirs. Several time-delay based reservoirs using discrete opto-electronic and all-optical components [2, 3] have been demonstrated before. Implementations of photonic reservoirs on integrated platforms, however, amount to only a few on active platforms [4].

Here we implement a photonic reservoir node on an integrated silicon nitride based nonlinear photonic device. Its nonlinear dynamics arise from the cavity-induced optical intensity-dependent Kerr effect. Its passive, all-optical nature endows high processing speed, which allows for time-delay reservoirs with fast virtual nodes, and low latency. We experimentally demonstrate two benchmark tasks using the reservoir node in a time-delay architecture: (i) a nonlinear autoregressive moving average (NARMA-10) time series prediction task with normalized root-mean-square error of 0.183, and (ii) a binary classification on an earthquake sensor time series dataset with an accuracy of 69%, both comparable to the best reported values [5, 6]. These results pave the way towards high-speed, low latency photonic computing using nonlinear photonic nodes.

2. Description of the reservoir node

Fig. 1(a) illustrates the design of the all-optical reservoir node. It is composed of a microring resonator (MRR) loaded on an arm of a Mach-Zehnder interferometer (MZI) after a Mach-Zehnder coupler (MZC). Its nonlinear operation mechanism is based on the nonlinear Kerr effect in the MRR, which manifests as a nonlinear phase response to optical light amplitude. This nonlinear phase translates to nonlinear transmission via the MZI. MZC behaves as a tunable coupler allowing further control of the interference at the MZI output thereby adding a degree of control of the device transfer function. The tunability of the device is accomplished via thermo-optic heaters on the MRR, MZI and MZC that allow for tuning amplitude and phase biases of the device, which together enable the programmability of the nonlinear dynamic operation [7].

The photonic chip was manufactured on a commercial silicon nitride foundry process at Ligentec, Switzerland with high-quality LPCVD technology. The waveguides are all 800 nm thick and 1 μm wide. The MRR has a radius of 50 μm with a 0.5 μm gap with the bus waveguide, and 0.51 μm with the drop waveguide. The arms of the interferometers have a length difference of 7 μm. Aluminum-based metal layer of 400 nm thickness is deposited atop the optical components as heaters and routing traces for thermo-optic device biasing. Inverted taper structures are used for edge-coupling TE mode into and off the chip.

3. Experimental procedure and results

A camera image, as well as schematic illustration of the experimental setup are shown in Figs. 1(b) and (c) respectively. Optical coupling into the photonic chip is through an array of ultra-high numerical aperture (UHNA)

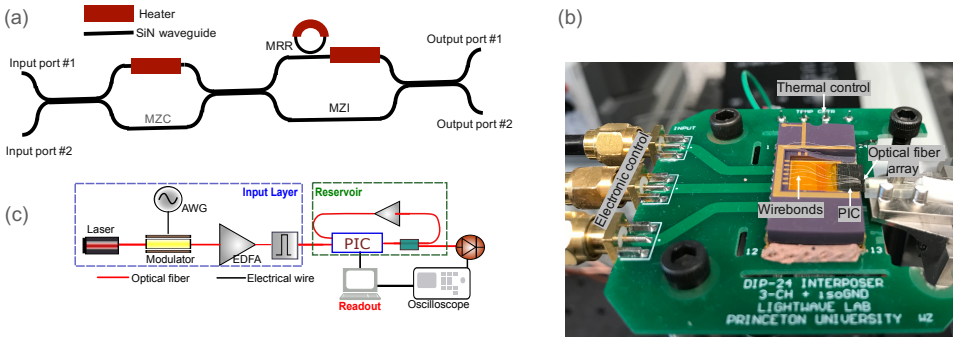

Fig. 1. (a) Schematic of the device, comprised of a microring resonator (MRR) and Mach-Zehnder interferometers (MZI and MZC) on SiN, and metal heaters for biasing, and the optical input/output ports. (b) Camera image of the probed photonic chip (PIC), showing the optical fiber array edge coupled to the chip, and well as the electrical wirebonds used for device biasing. (c) Schematic of the experimental setup, showing input generation, reservoir node and off-chip feedback and readout.

fibers edge coupled to the on-chip inverse tapers, resulting in an insertion loss of 5 dB/facet. Electronic control signals for the device biases are sent through standard SMA cables connected to PCB traces and wirebonds, which in turn connect to on-chip contact traces and device heaters (refer Fig.1(b)). The resistances of the heater pathways, including the contact traces, are approximately 100 Ω.

We experimentally demonstrate two benchmark tasks using a photonic reservoir implemented on the device in Fig. 1(a). The reservoir network architecture is shown in Figure 1(c). The input signal is programmed onto the AWG at a sampling rate of 36 GSa/s which then modulates the laser output. The modulated optical signal is then amplified by an EDFA and filtered by a bandpass filter. This is then fed as the input to the on-chip photonic reservoir with an average optical power of 9 dBm. The output of the photonic chip is split into two pathways: one of which feeds back into the PIC after being amplified to compensate for the chip-fiber coupling loss as the delay loop of the reservoir. The input and feedback signal power ratio was about 15:1. By tuning the device biases, the output of the photonic reservoir node is nonlinearly transformed. The output of the reservoir is captured by a real-time oscilloscope (50GSa/s) and sent to a computer. The details of the tasks and the reservoir architecture employed are outlined below:

- **NARMA-10 time series prediction:** The nonlinear autoregressive moving average model, i.e. NARMA-10, is often used as a benchmark task to compare recurrent neural network and reservoir models. Mathematically, the NARMA-10 series can be written as follows:

$$y_{n+1} = 0.3y_n + 0.05y_n \sum_{n=1}^{9} y_{n-1} + 1.5u_{n-9}u_n + 0.1 \quad (1)$$

  For the nth time step, u_n is a random input and y_n is the NARMA-10 output. In the experiment, first we generate a random input sequence u of length 1000 and the corresponding NARMA-10 series is calculated using Eq. 1. Then an input weight mask of length 200 is applied to the random input sequence u to generate a sequence of length 1000x200. This input data is sampled at 36 GSa/s by an AWG, resulting in reservoir virtual node spacing of 27 ps, which is then modulated onto an optical carrier and sent to the reservoir. 70% of the series is used for training and the remainder for testing. In the training stage, a ridge regression algorithm is applied to fit the output of the reservoir and the target NARMA-10 output, which gives us the readout weights of the reservoir. In the testing stage, those readout weights are applied to the optical output to obtain the network predicted output. Preliminary experimental results are shown in Fig. 3(a), where we achieve a normalized root mean square error of 0.183, which is comparable to [1] and better than other optical approaches [5]. We note that the network hyperparameters were not optimized for optimal accuracy, and better performance may be attainable.

- **Earthquake classification using time-series sensor data:** This task uses a dataset from the UCR time series archive that contains the sensor readings taken at the Northern California Earthquake Data Center from 1967 to 2003. It is a binary classification problem to classify positive and negative cases (as defined in Ref. [6]), containing 322 time series for training and 139 time series for testing, each of length 512. To implement this classification problem on the photonic reservoir, we first train the reservoir. We apply a random read-in weight matrix of size 512x100 to the input time series of size 322x512, resulting in a flattened time series of length 322x100. We pad in between consecutive input values with zeros such that there is no mixing between adjacent

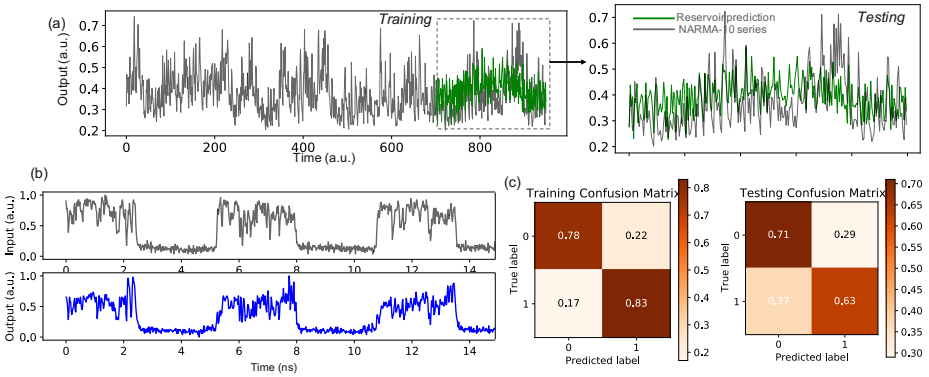

Fig. 2. Experimental results of (a) NARMA-10 prediction task, showing the photonic reservoir predicted output relayed onto the NARMA-10 time series of length 1000. The network was trained on 75% of the series, and tested on the remainder. and Binary earthquake classification problem: (b) sample reservoir input and output for 3 time series, (c) classification confusion matrices for training and testing.

time series, which results in an input sequence of time series as shown in Figure. (b). This input time-series is then fed into the photonic reservoir and the nonlinearly transformed output is recorded. A ridge classifier algorithm is then used to fit the reservoir output and the target classes to obtain the readout weights. Similarly, we then generate an input time series of the testing dataset of size 139x100, pad them with zeroes, and record the reservoir output. We then generate the reservoir predicted classes by applying the readout weights obtained during training onto the optical output. Figure (b) shows the reservoir input and the reservoir output time series sequence for a sample of 3. Figure (c) shows the confusion matrices of the classification problem during training and testing stages. Both the matrices are diagonal, as desired. The classification accuracies during training and testing were 78.9% and 69.1% respectively, which are only slightly below the best reported accuracy of 75.92% [6]. The network parameters were not optimized so a better performance may be achieved.

4. Conclusion

We report experimental results on a NARMA-10 time series prediction task, and a binary classification problem on earthquake sensor data using an integrated nonlinear photonic device as the reservoir node. This serves as a path towards employing nonlinear photonic neurons for high-speed, low-latency neural processing.

Acknowledgements

This research is supported by the Office of Naval Research (ONR) (N00014-18-1-2297). Device fabrication is credited to Ligentec in Switzerland.

References

1. L. Appeltant, M. C. Soriano, G. Van der Sande, J. Danckaert, S. Massar, J. Dambre, B. Schrauwen, C. R. Mirasso, and I. Fischer, "Information processing using a single dynamical node as complex system," Nat. communications **2**, 1–6 (2011).
2. Y. Paquot, F. Duport, A. Smerieri, J. Dambre, B. Schrauwen, M. Haelterman, and S. Massar, "Optoelectronic reservoir computing," Sci. reports **2**, 1–6 (2012).
3. K. Takano, C. Sugano, M. Inubushi, K. Yoshimura, S. Sunada, K. Kanno, and A. Uchida, "Compact reservoir computing with a photonic integrated circuit," Opt. express **26**, 29424–29439 (2018).
4. K. Harkhoe, G. Verschaffelt, A. Katumba, P. Bienstman, and G. Van der Sande, "Demonstrating delay-based reservoir computing using a compact photonic integrated chip," Opt. express **28**, 3086–3096 (2020).
5. Q. Vinckier, F. Duport, A. Smerieri, K. Vandoorne, P. Bienstman, M. Haelterman, and S. Massar, "High-performance photonic reservoir computer based on a coherently driven passive cavity," Optica **2**, 438–446 (2015).
6. H. A. Dau, A. Bagnall, K. Kamgar, C.-C. M. Yeh, Y. Zhu, S. Gharghabi, C. A. Ratanamahatana, and E. Keogh, "The ucr time series archive," IEEE/CAA J. Autom. Sinica **6**, 1293–1305 (2019).
7. C. Huang, A. Jha, T. F. De Lima, A. N. Tait, B. J. Shastri, and P. R. Prucnal, "On-chip programmable nonlinear optical signal processor and its applications," IEEE J. Sel. Top. Quantum Electron. **27**, 1–11 (2020).